Super Twisting Sliding Mode Controller for Trajectory Tracking Control of Autonomous Ground Vehicle System

Tamiru Takele[1(✉)], Tefera Terefe[2], and Sam Sun Ma[2]

[1] Wolaita Sodo University, Sodo, Ethiopia
tamirutakele001@gmail.com
[2] Electrical Power and Control Engineering, Adama Science and Technology University, Adama, Ethiopia

Abstract. Day to day increase in demand of safe and accident free ground vehicle, rapid growth and development of artificial intelligence algorithms and also rapid growth of microelectronics technology are major motives that are driving the development and increased attention of Autonomous Ground Vehicle (AGV) systems. Unstable and non-linear features of AGV need robust control techniques to control the trajectory tracking tasks of the system. Review of related works summery shows that sliding mode controller can handle non-linearity and relatively assure robustness of the system. However; ripple is one of the most common challenge in sliding mode controllers. In this research, Super Twisting Sliding Mode controller (STSMC) is designed to resolve the ripple in sliding mode controller for trajectory tracking control of AGV. Optimal parameters of STSMC controller are tuned using Genetic Algorithm (GA) and Particle Swarm Optimization (PSO) technique. To compare the performance of the proposed algorithm, GA tuned Fractional-Order-PID (FOPID) controller is also designed and implemented. Accordingly, STSMC has less (≈0.0006 s) tracking error than FOPID controller. The result reveals the outperformance of the proposed algorithm over FOPID controller.

Keywords: Autonomous Ground Vehicle · Trajectory tracking · Super Twisting Sliding Mode Controller · Fractional order proportional integral derivative controller · Optimization algorithms

1 Introduction

1.1 Background

A ground vehicle that can travel in both structured and unstructured situations without constant human guidance is referred to as an autonomous ground vehicle (AGV), also known as an intelligent vehicle. Autonomous vehicle systems may vary depending on the environment in which they are used. Unmanned aerial vehicles (UAVs), also referred to as flying and aerial vehicles (FAVs), are autonomous vehicles that fly higher than the

B. H. Woldegiorgis et al. (Eds.): ICAST 2022, LNICST 455, pp. 272–289, 2023.
https://doi.org/10.1007/978-3-031-28725-1_17

ground. There are also unmanned and autonomous vehicles operating below sea level which also known as unmanned underwater vehicle (UUV) [1]. This paper focuses on self-driving vehicles that operate on the ground, also known as AGV.

On its route to a target, which can be a single spot, a region, or a trajectory of sites, an AGV can recognize and avoid impediments. The complexity of today's transportation systems makes management and security more challenging to guarantee. Due to the exponential growth in the number of vehicles on the road, fundamental human behaviors are now fraught with danger. This issue may be solved by autonomous vehicles that take the role of human drivers. Mobile robots (car-like vehicles or autonomous vehicles) are able to carry out a range of tasks in hazardous environments where humans are unable to enter, such as those sites where harmful gases or high temperatures exist in a harsh environment for humans. They can also use autonomous vehicles to ensure the delivery of goods over long distances on hazardous roads. We can save money by doing a variety of mundane jobs, [2]. The difficulty of tracking the trajectory of an autonomous ground vehicle (AGV) has received a lot of attention lately. Due to the quick advancement of autonomous vehicles, autonomous vehicle control is becoming more and more important in the field of vehicle autonomy research. As a result, it's critical to upgrade and improve autonomous vehicle controllers in order to accomplish this goal. These controllers must be able to handle complicated problems in a range of environments. At the lower level of control, autonomous vehicles can also move laterally and longitudinally. The noteworthy adaptive cruise control (ACC) and the more sophisticated cooperative adaptive cruise control (CACC) are examples of longitudinal control that concentrate on speed control, whereas lateral control handles path following and vehicle steering control [3]. The goal of this study is to better trajectory track and follow performance by looking into steering control methods for autonomous vehicles.

PID controllers have been used to control several industrial processes all over the world for a very long time. The Ziegler-Nichols method, genetic algorithm GA, fuzzy logic controller, and others are among the most well-known and often used techniques for altering the PID controller parameters in line with changes in the state of the environment and the system. The PSO optimization algorithm was another widely used tuning approach [4].

1.2 Literature Review

This section provides a summary of previous attempts to develop AGV controllers. When first building an AGV controller, the knowledge gained from reading various scientific articles and publications is very valuable. Many academics have recently developed route tracking control algorithms that take into account the non-holonomic constraints that an AGV must follow. In [5], By creating a Lyapunov function, a kinematic controller for the mobile platform was generated to achieve the necessary velocity. Also suggested was a stable adaptive tracking controller. According to Lyapunov stability theory, the designed robust adaptive controller assures overall stability of the closed-loop system. In [6], An innovative control technique for following the path of mobile robots was developed by Zhang. An international finite-time angular velocity control law was used to design this control technique. According to the simulation results, mobile robot angle errors can be stabilized with good convergence and performance. In [7], Wang developed an adaptive

trajectory tracking approach based on the kinematics model to solve the non-holonomic restriction problem of trajectory tracking of the wheeled mobile robot. This technique builds based on the idea of an artificial field to improve trajectory tracking.

In [8], For the path tracking issue of a mobile robot, Normey developed a traditional PID controller. The resilience of the closed-loop system was taken into consideration as a new PID tuning technique based on fundamental control tools was proposed. In [9], Lee and Chang proposed two strategies for improving a FOPID controller. These techniques employ electromagnetism and evolutionary algorithms. In order to incorporate the advantages of both approaches while lessening the computational load on the electromagnetic algorithm, a hybrid approach was created.

In [10], Using adaptive PID control, P. Zhao introduced and discussed the design of the "intelligent pioneer" autonomous vehicle's control system, as well as path tracking and motion stability. The experimental implementation of trajectory control of the mobile robots is presented in [11] considering the dynamics of their subsystems. Taking in to account subsystem dynamics is benefit what I gained from it. The Particle Swarm Optimization approach is used in [12] to create fractional order PID controllers that outperform its integer order counterparts. The requisite peak overshoot and rising time specifications form the basis for controller synthesis. By minimizing the characteristic equation, the ideal set of controller parameters is obtained. In [13] Under difficult conditions like as nonlinearity, strong coupling, high uncertainties, and disturbances, an Adaptive Super Twisting Sliding Mode (ASTSM) Control method is used to control quadcopter attitudes. It deals with the modeling and control of unmanned aerial vehicles such as quadcopters and drones (UAVs). The Adaptive Super Twisting Sliding Mode controller may accomplish robust operation with disturbance rejection, parametric variation adaption, and chattering attenuation, according to simulation results.

AGV Trajectory Tracking Control of the lateral dynamics model of the vehicle is created using a Genetic Algorithm based on the bicycle model is proposed in [14], in which PID parameters are optimized by genetic algorithms. The simulation results demonstrate that even in the presence of outside disturbance, the developed PID controller has good tracking capability. In [15] AGV Path Tracking Use a Fractional Order Extremum Seeking Controller (FO-ESC) to control a non-holonomic autonomous ground vehicle while monitoring its behavior along a predetermined reference path.

In general, the majority of their works in the above literature study track the behavior of the preset reference path for the AGV. Some of them used optimization techniques as well as checking the tracking performance even in the presence of external disturbance. Even if their work follows the behavior of a predefined reference path, their tracking performance and error minimization technique aren't very good. As a result, this research proposes utilizing an STSMC controller with a genetic algorithm and particle swarm optimization approaches to reduce performance error and manage the orientation and velocity of the AGV.

2 Mathematical Modelling of Lateral Vehicle Dynamics Based on Bicycle Model

As indicated in Fig. 1, a bicycle model of the vehicle with two degrees of freedom is studied [10]. The two degrees of freedom are represented by the vehicle lateral position

y and the vehicle yaw angle ψ. The vehicle lateral position is measured along the lateral axis of the vehicle to the point O which is the center of rotation of the vehicle. The vehicle yaw angle is measured with respect to the global X axis. The longitudinal velocity of the vehicle at the center of gravity is represented by V_x.

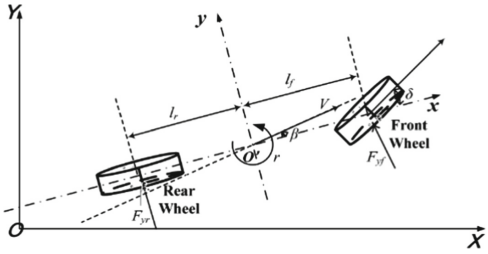

Fig. 1. Equivalent bicycle model

Newton's second law is used to describe motion along y axis.

$$ma_y = F_{yf} + F_{yr} \tag{1}$$

where $a_y = d^2y/dt^2$ is the direction that the vehicle's inertial acceleration at c.g. of the y axis. F_{yf} and F_{yr} are the lateral tire forces of the front and rear wheels respectively. Two terms contribute to a_y: the acceleration $\ddot{y}$ which is due to motion along the y axis and the centripetal acceleration $V_x\dot{\psi}$.

Hence,

$$a_y = \ddot{y} + V_x\dot{\psi} \tag{2}$$

Substituting from Eq. (2) into Eq. (1), the equation for the vehicle's lateral translational motion is as follows:

$$m\left(\ddot{y} + V_x\dot{\psi}\right) = F_{yf} + F_{yr} \tag{3}$$

The equation for the yaw dynamics is given by moment balance about the z axis as

$$I_z\ddot{\psi} = l_fF_{yf} - l_rF_{yr} \tag{4}$$

where l_f and l_r are the separations between the front and rear tires in relation to the center of gravity of the vehicle. To model the lateral tire forces F_{yf} and F_{yr} that act on the vehicle; the lateral tire force of a tire is proportional to the "slip-angle" for small slip-angles. The angle between the orientation of the tire and the orientation of the wheel's velocity vector is known as the slip angle of a tire. The slip angle of the front wheel is:

$$\alpha_f = \delta - \theta_{vf} \tag{5}$$

where θ_{vf} is the angle that the vehicle's longitudinal axis and the velocity vector make and δ is the front wheel steering angles. The rear slip angle is similarly given by:

$$\alpha_r = -\theta_{vr} \tag{6}$$

Therefore, the lateral tire force for the vehicle's front wheels can be written as

$$F_{yf} = 2C_{af}(\delta - \theta_{vf}) \tag{7}$$

where the proportionality constant C_{af} is called the front tire cornering stiffness

The lateral tire for the back wheels can be expressed similarly as

$$F_{yr} = 2C_{ar}(-\theta_{vr}) \tag{8}$$

where C_{ar} the rear tire cornering stiffness and θ_{vr} is the rear tire velocity angle. The following relations can be used to calculate θ_{vf} and θ_{vr}:

$$\begin{cases} \tan(\theta_{vf}) = \dfrac{V_y + l_f\dot{\psi}}{V_x} \\ \tan(\theta_{vr}) = \dfrac{V_y - l_r\dot{\psi}}{V_x} \end{cases} \tag{9}$$

Using the notation and small angle approximation $V_y = \dot{y}$

$$\begin{cases} \theta_{vf} = \dfrac{\dot{y} + l_f\dot{\psi}}{V_x} \\ \theta_{vr} = \dfrac{\dot{y} - l_f\dot{\psi}}{V_x} \end{cases} \tag{10}$$

Substituting from Eqs. (5), (6), (9) and (10) into Eqs. (3) and (4), the state space model can be written as

$$\frac{d}{dt}\begin{bmatrix} y \\ \dot{y} \\ \psi \\ \dot{\psi} \end{bmatrix} = \begin{bmatrix} 0 & 1 & 0 & 0 \\ 0 & -\frac{2C_{af}+2C_{ar}}{mV_x} & 0 & -V_x - \frac{2C_{af}l_f - 2C_{ar}l_r}{mVx} \\ 0 & 0 & 0 & 1 \\ 0 & -\frac{2l_fC_{af} - 2l_rC_{ar}}{I_zV_x} & 0 & -\frac{2l_f^2C_{af} + 2l_r^2C_{ar}}{I_zV_x} \end{bmatrix} + \begin{bmatrix} 0 \\ \frac{2C_{af}}{m} \\ 0 \\ \frac{2l_fC_{af}}{I_z} \end{bmatrix}\delta \tag{11}$$

As a result, the lateral model created by the aforementioned equations will be redefined in terms of the state error variables: x_1, the separation between the vehicle's center of gravity and the lane centerline; and x_2, a vehicle's position in relation to the road.

Take into account a car that is moving at a constant longitudinal velocity V_x on a road of constant radius. Define $\ddot{x}_1$ and x_2 as follows

$$\ddot{x}_1 = \left(\ddot{y} + V_x\dot{\psi}\right) - \frac{V_x^2}{R} = \ddot{y} + V_x\left(\dot{\psi} - \dot{\psi}_d\right) \tag{12}$$

And

$$x_2 = \psi - \psi_d \tag{13}$$

Define

$$\dot{x}_1 = \dot{y} + V_x(\psi - \psi_d) \tag{14}$$

Equation (14) is consistent with Eq. (12) if the velocity is constant. Hence the approach taken is to assume the longitudinal velocity is constant and obtain a LTI model. Substituting from Eqs. (15) and (16) into (3) and (4), we find

$$m\ddot{x}_1 = \dot{x}_1\left[-\frac{2}{V_x}C_{af} - \frac{2}{V_x}C_{ar}\right] + x_2[2C_{af} + 2C_{ar}] + \dot{x}_2\left[-\frac{2C_{af}l_f}{V_x} + \frac{2C_{ar}l_r}{V_x}\right] + \dot{\psi}_d\left[-\frac{2C_{af}l_f}{V_x} + \frac{2C_{ar}l_r}{V_x}\right] + 2C_{af}\delta \tag{15}$$

And

$$I_z\ddot{x}_2 = 2C_{af}l_f\delta + \dot{x}_1\left[-\frac{2C_{af}l_f}{V_x} + \frac{2C_{ar}l_r}{V_x}\right] + x_2[2C_{af}l_f - 2C_{ar}l_r] + \dot{x}_2\left[-\frac{2C_{af}l_f^2}{V_x} - \frac{2C_{ar}l_r^2}{V_x}\right] - I_z\ddot{\psi}_d + \dot{\psi}_d\left[-\frac{2C_{af}l_f^2}{V_x} - \frac{2C_{af}l_r^2}{V_x}\right] \tag{16}$$

The state space model in tracking error variables is therefore given by

$$\frac{d}{dt}\begin{bmatrix} x_1 \\ \dot{x}_1 \\ x_2 \\ \dot{x}_2 \end{bmatrix} = \begin{bmatrix} 0 & 1 & 0 & 0 \\ 0 & -\frac{2C_{af}+2C_{ar}}{mV_x} & \frac{2C_{af}+2C_{ar}}{m} & \frac{-2C_{af}l_f+2C_{ar}l_r}{mV_x} \\ 0 & 0 & 0 & 1 \\ 0 & -\frac{2C_{af}l_f-2C_{ar}}{I_zV_x} & \frac{2C_{af}l_f-C_{ar}l_r}{I_z} & -\frac{2C_{af}l_f^2+2C_{ar}l_r^2}{I_zV_x} \end{bmatrix}\begin{bmatrix} x_1 \\ \dot{x}_1 \\ x_2 \\ \dot{x}_2 \end{bmatrix} + \begin{bmatrix} 0 & 0 \\ \frac{2C_{af}}{m} & -\frac{2C_{af}l_f-2C_{ar}l_r}{mV_x} - V_x \\ 0 & 0 \\ \frac{2C_{af}l_f}{I_z} & -\frac{2C_{af}l_f^2+2C_{ar}l_r^2}{I_zV_x} \end{bmatrix}\begin{bmatrix} \delta \\ \dot{\psi}_d \end{bmatrix} \tag{17}$$

Note that the longitudinal vehicle speed, which has been assumed to be constant, determines how the lateral dynamics model is calculated. The state space model in Eq. (17) is in the form of $\dot{X} = Ax + Bu$ where:

$$A = \begin{bmatrix} 0 & 1 & 0 & 0 \\ 0 & a_{22} & a_{23} & a_{24} \\ 0 & 0 & 0 & 1 \\ 0 & a_{42} & a_{43} & a_{44} \end{bmatrix} \text{ and } B = \begin{bmatrix} 0 & 0 \\ b_{21} & b_{22} \\ 0 & 0 \\ b_{41} & b_{42} \end{bmatrix} \tag{18}$$

$$x = \begin{bmatrix} x_1 & \dot{x}_1 & x_2 & \dot{x}_2 \end{bmatrix}^T \text{ and } u = \begin{bmatrix} \delta & \dot{\psi}_d \end{bmatrix}^T \tag{19}$$

Therefore, the dynamic equation also becomes (Table 1)

$$\begin{cases} \dot{x}_1 = \dot{x}_1 \\ \ddot{x}_1 = a_{22}\dot{x}_1 + a_{23}\dot{x}_2 + a_{24}\dot{x}_2 + b_{21}\delta + b_{22}\dot{\psi}_d \\ \dot{x}_2 = \dot{x}_2 \\ \ddot{x}_2 = a_{42}\dot{x}_1 + a_{43}x_2 + a_{44}\dot{x}_2 + b_{41}\delta + b_{42}\dot{\psi}_d \end{cases} \tag{20}$$

$$\text{where, } a_{22} = \left[\frac{-2C_{af} + 2C_{ar}}{mV_x}\right], a_{23} = \left[\frac{2C_{af} + 2C_{ar}}{m}\right],$$

$$a_{24} = \left[\frac{-2C_{af}l_f + 2C_{ar}l_r}{mV_x}\right]$$

$$a_{42} = \left[\frac{-2C_{af}l_f - 2C_{ar}}{I_z V_x}\right], a_{43} = \left[\frac{2C_{af}l_f - C_{ar}l_r}{I_z}\right],$$
$$a_{44} = \left[\frac{-2C_{af}l_f^2 + 2C_{ar}l_r^2}{I_z V_x}\right]$$
$$b_{21} = \left[\frac{2C_{af}}{m}\right], b_{22} = \left[\frac{-2C_{af}l_f - 2C_{ar}l_r}{mV_x} - V_x\right]$$
$$b_{41} = \left[\frac{2C_{af}l_f}{I_z}\right], b_{42} = \left[\frac{-2C_{af}l_f^2 + 2C_{ar}l_r^2}{I_z V_x}\right]$$

Table 1. Technical specification for the AGV used for evaluation

Parameters	Description	Value	Unit
m	Mass of the vehicle	1573	Kg
I	Yaw moment of inertia	2873	Kgm^2
l_f	Distance from vehicle c.g to the front axis center	1.1	m
l_r	Distance from vehicle c.g to the front axis center	1.58	m
V_x	Longitudinal velocity of the vehicle	30	m/s
C_{af}	Cornering stiffness of front tire	80000	N/rad
C_{ar}	Cornering stiffness of rear tire	80000	N/rad

3 Controller Design

3.1 Sliding Mode Controller

This control method is based on the idea that the configuration of the controller should be changed frequently to maintain the state variables on the sliding manifold [16, 17]. Design of the sliding surface and design of the control input are two distinct stages of the Sliding Mode Controller (SMC) synthesis. The construction of the sliding surface is recognized as the most important stage in the development of the SMC because it is necessary to respond to the intended control requirements and performances. We should select the sliding surfaces before designing SMC. Surface types like PD, PI, and PID may be included in the surface. Similar SMC sliding surfaces were used in the construction of the STSMC controller.

3.2 Super Twisting Sliding Mode Controller

The main drawback of first order sliding mode controller is chattering. The discontinuous control signal that results from the system variables oscillating around the sliding surface causes this phenomena. This effect might damage or disturb the physical system. Using HOSM is one of the more exciting ways to eliminate or reduce the chattering effect. The higher order temporal derivatives of the sliding surface are kept to zero in this technique [21]. As a result, the chattering impact is reduced as a result of this activity. However, the fundamental issue in implementing HOSM algorithms is the growing information need. Thus;

$$U = u_{eq} + u_c \tag{21}$$

For this system controller design choosing the PD surface as:

$$S_1 = C_1 e_1 + \dot{e}_1 \tag{22}$$

where C1 is a sliding constant and e1 and ė1 are the error and error derivative respectively. Since $u(t) = k_p e(t) + k_d \frac{d}{dt} e(t)$

Let us define the errors as

$$e_1 = x_{1d} - x_1 \tag{23}$$

$$\dot{e}_1 = \dot{x}_{1d} - \dot{x}_1 \tag{24}$$

$$\ddot{e}_1 = \ddot{x}_{1d} - \ddot{x}_1 \tag{25}$$

Differentiating the surface S1 of Eq. (22)

$$\dot{S}_1 = C_1 \dot{e}_1 + \ddot{e}_1 \tag{26}$$

Inserting Eq. (24) and (25) in Eq. (26)

$$\dot{S}_1 = C_1(\dot{x}_{1d} - \dot{x}_1) + (\ddot{x}_{1d} - \ddot{x}_1) \tag{27}$$

Inserting Eq. (20) in Eq. (27)

$$\dot{S}_1 = C_1(\dot{x}_{1d} - \dot{x}_1) + \left(\ddot{x}_{1d} - a_{22}\dot{x}_1 - a_{23}x_2 - a_{24}\dot{x}_2 - b_{21}\delta - b_{22}\dot{\psi}_d\right) \tag{28}$$

The Lyapunov theorem, a well-known approach in stability research, is used to validate the steady convergence behavior of nonlinear controllers [18–20]. We can use the Lyapunov function to demonstrate the stability as in Eq. (29) with its time derivative given in Eq. (30).

$$V = \frac{1}{2}s^2 \tag{29}$$

$$\dot{V} = s\dot{s} \tag{30}$$

With $V = 0$ and $V > 0$ for $s \neq 0$. The following reaching criterion must be adhered to in order to guarantee that the trajectory transitions from the reaching to the sliding phase while maintaining stability:

$$\dot{V} < 0, \text{ for } s \neq 0, \dot{s} \neq 0 \tag{31}$$

For $S_1\dot{S}_1 \leq 0$ Eq. (28) becomes

$$C_1(\dot{x}_{1d} - \dot{x}_1) + \left(\ddot{x}_{1d} - a_{22}\dot{x}_1 - a_{23}x_2 - a_{24}\dot{x}_2 - b_{21}\delta - b_{22}\dot{\psi}_d\right) = 0 \tag{32}$$

$$C_1(\dot{x}_{1d} - \dot{x}_1) + (\ddot{x}_{1d} - a_{22}\dot{x}_1 - a_{23}x_2 - a_{24}\dot{x}_2) = b_{21}\delta + b_{22}\dot{\psi}_d \tag{33}$$

Letting $b_{22} = 0$ Eq. (33) becomes

$$C_1(\dot{x}_{1d} - \dot{x}_1) + (\ddot{x}_{1d} - a_{22}\dot{x}_1 - a_{23}x_2 - a_{24}\dot{x}_2) = b_{21}\delta \tag{34}$$

$$\delta = \frac{C_1(\dot{x}_{1d} - \dot{x}_1) + (\ddot{x}_{1d} - a_{22}\dot{x}_1 - a_{23}x_2 - a_{24}\dot{x}_2)}{b_{21}} \tag{35}$$

Letting $b_{21} = 0$ Eq. (33) becomes

$$C_1(\dot{x}_{1d} - \dot{x}_1) + (\ddot{x}_{1d} - a_{22}\dot{x}_1 - a_{23}x_2 - a_{24}\dot{x}_2) = b_{22}\dot{\psi}_d \tag{36}$$

$$\dot{\psi}_d = \frac{C_1(\dot{x}_{1d} - \dot{x}_1) + (\ddot{x}_{1d} - a_{22}\dot{x}_1 - a_{23}x_2 - a_{24}\dot{x}_2)}{b22} \tag{37}$$

Now letting:

$$u_{eq1} = \delta + \dot{\psi}_d \tag{38}$$

$$u_{eq1} = \left[\frac{b_{21} + b_{22}}{b_{21}b_{22}}\right](C_1(\dot{x}_{1d} - \dot{x}_1) + (\ddot{x}_{1d} - a_{22}\dot{x}_1 - a_{23}x_2 - a_{24}\dot{x}_2)) \tag{39}$$

For second controller, choosing the sliding surface two:

$$S_2 = C_2e_2 + \dot{e}_2 \tag{40}$$

Let us also define the errors as

$$e_2 = x_{2d} - x_2 \tag{41}$$

$$\dot{e}_2 = \dot{x}_{2d} - \dot{x}_2 \tag{42}$$

$$\ddot{e}_2 = \ddot{x}_{2d} - \ddot{x}_2 \tag{43}$$

Differentiating the surface S2 of Eq. (40)

$$\dot{S}_2 = C_2\dot{e}_2 + \ddot{e}_2 \tag{44}$$

Inserting Eq. (42) and (43) in Eq. (44)

$$\dot{S}_2 = C_2(\dot{x}_{2d} - \dot{x}_2) + (\ddot{x}_{2d} - \ddot{x}_2) \tag{45}$$

Inserting Eq. (20) in Eq. (45)

$$\dot{S}_2 = C_2(\dot{x}_{2d} - \dot{x}_2) + \left(\ddot{x}_{2d} - a_{42}\dot{x}_1 - a_{43}x_2 - a_{44}\dot{x}_2 - b_{41}\delta - b_{42}\dot{\psi}_d\right) \tag{46}$$

For $S_2\dot{S}_2 \leq 0$ Eq. (46) becomes

$$C_2(\dot{x}_{2d} - \dot{x}_2) + \left(\ddot{x}_{2d} - a_{22}\dot{x}_1 - a_{23}x_2 - a_{24}\dot{x}_2 - b_{41}\delta - b_{42}\dot{\psi}_d\right) = 0 \tag{47}$$

$$C_1(\dot{x}_{2d} - \dot{x}_2) + (\ddot{x}_{2d} - a_{42}\dot{x}_1 - a_{43}x_2 - a_{44}\dot{x}_2) = b_{41}\delta + b_{42}\dot{\psi}_d \tag{48}$$

Letting the parameter $b_{42} = 0$ in Eq. (47) becomes

$$C_2(\dot{x}_{2d} - \dot{x}_2) + (\ddot{x}_{2d} - a_{42}\dot{x}_1 - a_{43}x_2 - a_{44}\dot{x}_2) = b_{41}\delta \tag{49}$$

$$\delta = \frac{C_2(\dot{x}_{2d} - \dot{x}_2) + (\ddot{x}_{2d} - a_{42}\dot{x}_1 - a_{43}x_2 - a_{44}\dot{x}_2)}{b_{41}} \tag{50}$$

Letting the parameter $b_{41} = 0$ in Eq. (48) becomes

$$C_2(\dot{x}_{2d} - \dot{x}_2) + (\ddot{x}_{2d} - a_{42}\dot{x}_1 - a_{43}x_2 - a_{44}\dot{x}_2) = b_{42}\dot{\psi}_d \tag{51}$$

$$\dot{\psi}_d = \frac{C_2(\dot{x}_{2d} - \dot{x}_2) + (\ddot{x}_{2d} - a_{42}\dot{x}_1 - a_{43}x_2 - a_{44}\dot{x}_2)}{b42} \tag{52}$$

Now letting:

$$u_{eq2} = \delta + \dot{\psi}_d \tag{53}$$

$$u_{eq2} = \left[\frac{b_{41} + b_{42}}{b_{41}b_{42}}\right](C_2(\dot{x}_{2d} - \dot{x}_2) + (\ddot{x}_{2d} - a_{42}\dot{x}_1 - a_{43}x_2 - a_{44}\dot{x}_2)) \tag{54}$$

For STSMC;

$$u_c = -K_1|\sqrt{s}|\text{sgn}(s) - K_2\int_0^t \text{sgn}(s)dt \tag{55}$$

Therefore, the controller for STSMC1 designed as,

$$U_1 = u_{eq1} + u_c \tag{56}$$

Inserting Eq. (39) and (55) in Eq. (60) becomes,

$$U_1 = \left[\frac{b_{21} + b_{22}}{b_{21}b_{22}}\right](C_1(\dot{x}_{1d} - \dot{x}_1) + (\ddot{x}_{1d} - a_{22}\dot{x}_1 - a_{23}x_2 - a_{24}\dot{x}_2)) + \left(-K_1|\sqrt{s}|\text{sgn}(s) - K_2\int_0^t \text{sgn}(s)dt\right) \tag{57}$$

Therefore, the controller for STSMC2 designed as,

$$U_2 = u_{eq2} + u_c \tag{58}$$

Inserting Eq. (54) and (55) in Eq. (62) becomes,

$$U_2 = \left[\frac{b_{41} + b_{42}}{b_{41}b_{42}}\right](C_2(\dot{x}_{2d} - \dot{x}_2) + (\ddot{x}_{2d} - a_{42}\dot{x}_1 - a_{43}x_2 - a_{44}\dot{x}_2)) + \left(-K_1|\sqrt{s}|\text{sgn}(s) - K_2\int_0^t \text{sgn}(s)dt\right) \tag{59}$$

3.3 Fractional Order PID Controller

Fractional-order proportional-integral-derivative (FOPID) controllers have attracted a lot of attention in recent years from both academia and industry. Because they have five parameter options, they actually provide greater design flexibility than typical PID controllers (instead of three). This does however imply that adjusting the controller might be much more difficult. The integral-differential equation describes the control action of a fractional-order PID controller as follows:

$$u(t) = k_p e(t) + k_i D_t^{-\lambda} e(t) + k_d D_t^{\mu} e(t) \tag{60}$$

FOPID's transfer function is obtained by applying the Laplace transform as follows (Fig. 2):

$$U(s) = k_p + k_i s^{-\lambda} + k_d s^{\mu} \tag{61}$$

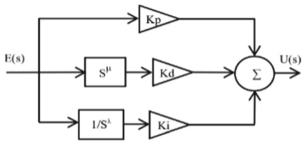

Fig. 2. The fractional order controller block diagram

Objective Functions

The Defining an objective function is one of the major tasks while formulating a problem using an optimization algorithm. The sum of two objective cost functions is the cost function that minimizes the system's error, because the proposed autonomous ground vehicle system is a multiple input multiple output system [22], written as:

$$\mathrm{J} = \mathrm{ITAE} = \int_0^{\tau} \mathrm{t}(|\mathrm{e}_1(\mathrm{t})| + |\mathrm{e}_2(\mathrm{t})|)\mathrm{d}\tau \tag{62}$$

whereas, $\mathrm{e}_1(\mathrm{t}) = \delta_{\mathrm{ref}} - \delta_{\mathrm{act}}$ and $\mathrm{e}_2(\mathrm{t}) = \dot{\psi}_{\mathrm{dref}} - \dot{\psi}_{\mathrm{dact}}$. Where δ orientation angle and $\dot{\psi}_{\mathrm{d}}$ is velocity.

4 Results and Discussions

4.1 MATLAB Implementations

The Matlab Simulink is used to design and simulate the proposed system mathematical model and controller design (Fig. 3).

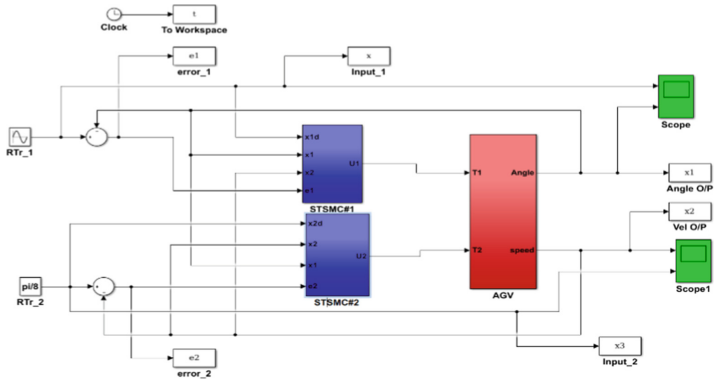

Fig. 3. The Simulink model of the proposed system STSMC

4.2 Open Loop Response

For a given step and constant input the system the open loop response output is highly nonlinear and unstable. The open loop response of the proposed system is shown as in Fig. 4 below:

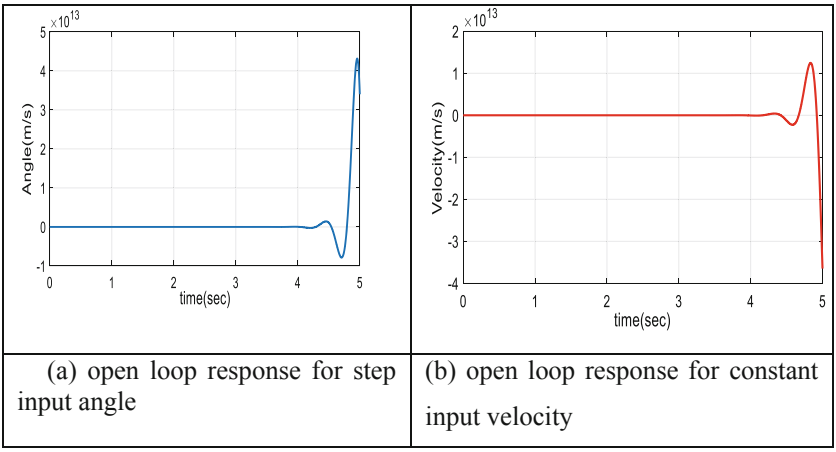

(a) open loop response for step input angle

(b) open loop response for constant input velocity

Fig. 4. Open loop response of the proposed system

4.3 Testing of Trajectories for Closed Loop Responses

After the model of the autonomous ground vehicle and the two STSMC controllers have been deployed, several case studies are used to simulate and examine the various trajectories in order to compare how the suggested technique responds to the FOPID controller. Each instance requires a distinct strategy, as can be seen below:

Test Case-1
A sinusoidal trajectory was created in this instance as a reference trajectory. Whereas, reference trajectory input is $\delta_d = 5\sin(t)$. To determine the orientation and velocity inaccuracy, this trajectory was compared to the real trajectory. As a result, the STSMC controller received the error. The STSMC1 controller's output offers the control action that was linked to the left wheel's motor. The second input serves as a representation of the intended velocity. The actual speed of the vehicle was contrasted with this speed. The error that was made when comparing the velocity was sent to the second STSMC2 controller. The velocity controller's output was coupled to the right wheel's motor. Figure 5 shows the relationship between the desired and actual trajectory after performing the simulation. As seen in Fig. 5, the system tracks the sinusoidal reference trajectory very well. Figure 7 shows the difference between the desired and actual orientation angle and velocity (Fig. 6).

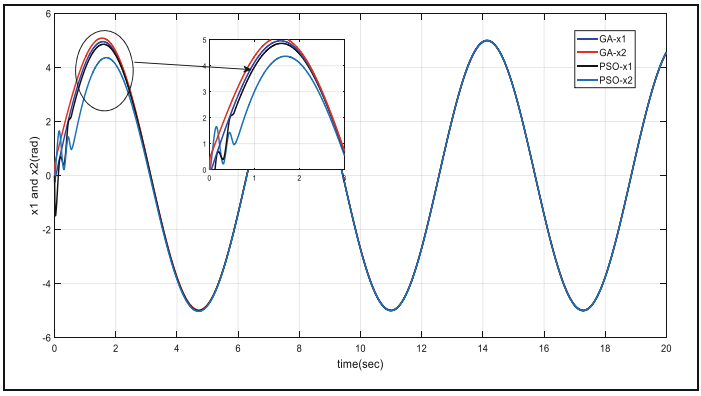

Fig. 5. The orientation response for a sinusoidal trajectory $\delta_d = 5\sin(t)$ proposed system

Test Case-2
In response to a different scenario and to show how flexible the suggested controller is, a linear trajectory was created. Creating a constant orientation will guarantee a linear trajectory using $\delta_d = \pi/4$ for interval $0 \leq t \leq 20$ s. Similarly, Figs. 8a and 8b illustrate the connection between the desired and actual trajectories. Figure 10 shows the difference in direction and velocity between the desired and actual values.

In Table 2 the error performance analysis of sinusoidal trajectory $\delta_d = 5\sin(t)$, we can say that the proposed STSMC controller has better error performance for PSO

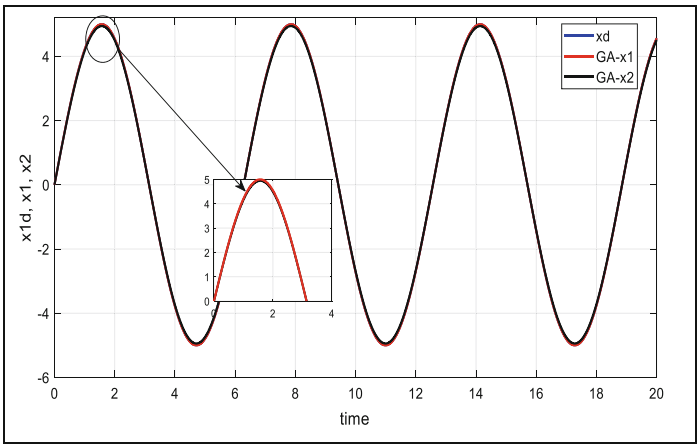

Fig. 6. Orientation angle and velocity response for sinusoidal trajectory $\delta_d = 5\sin(t)$ of FOPID controller

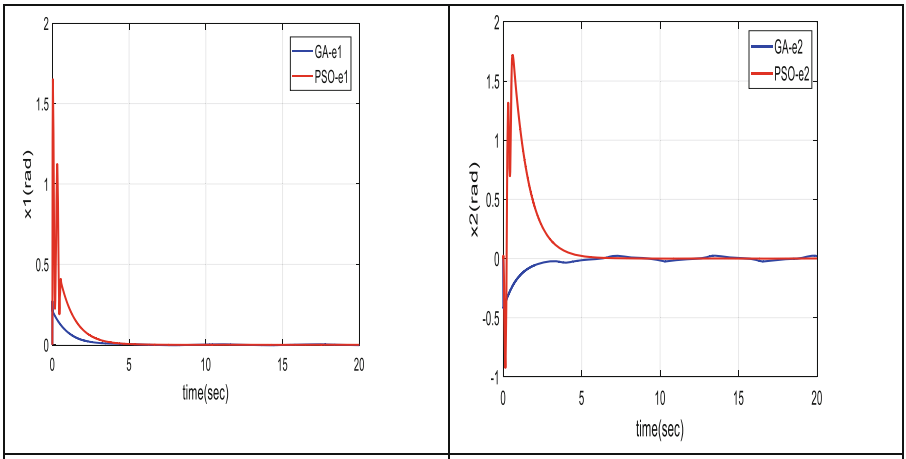

a) Orientation angle error response for STSMC

b) Velocity error response for STSMC

Fig. 7. Orientation angle and velocity error for sinusoidal trajectory $\delta_d = 5\sin(t)$ of STSMC

optimazation technique than GA based for both orientation angle and velocity control. And the error performance of proposed STSMC controller is much better than GA based FOPID controller for angle and velocity control. Adding disturbances due to friction of wheels during vehicle motion which is formed by varying the cornering stiffness value $C_{af} = C_{ar} = 40000$ N/rad and mass of 1500 kg has the orientation angle and velocity error 0.0004 and 0.0008 s respectively for sinusoidal trajectory of proposed PSO-based STSMC controllers (Fig. 9).

Table 2. The error performance analysis of the trajectory $\delta_d = 5\sin(t)$

Controllers	Angle error	Velocity error
GA-based STSMC	0.0026	0.0212
PSO-based STSMC	0.0006	0.0007
GA-based STSMC	0.0030	0.0538

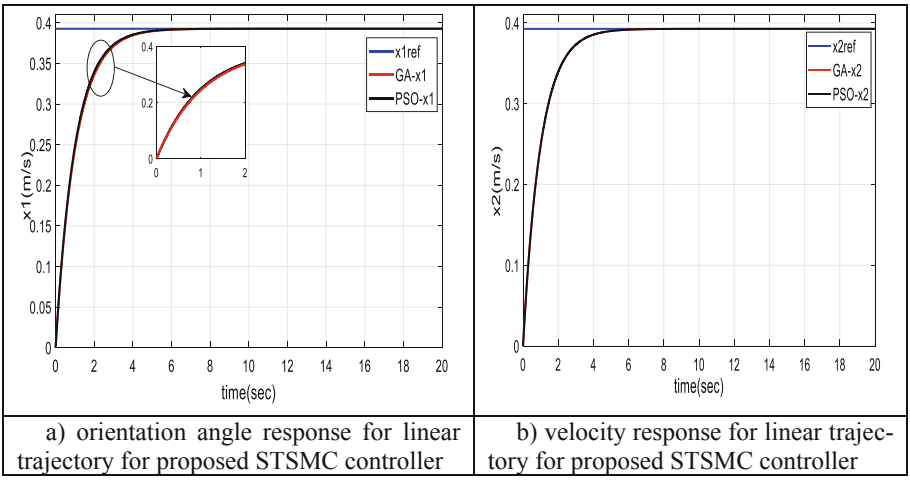

a) orientation angle response for linear trajectory for proposed STSMC controller

b) velocity response for linear trajectory for proposed STSMC controller

Fig. 8. The orientation angle and velocity response for linear trajectory $\delta_d = \pi/4$

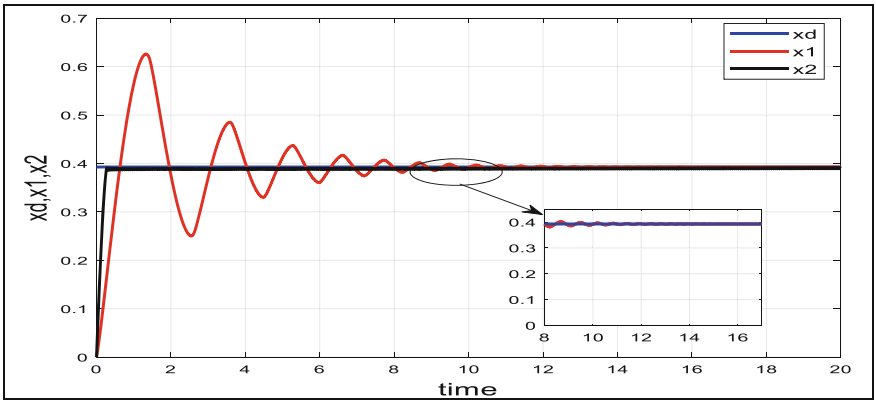

Fig. 9. The orientation angle and velocity response for linear trajectory $\delta_d = \pi/8$ of FOPID controller

As depicted in Fig. 10a for a linear trajectory of an orientation and velocity error response highly converges to zero for both GA and PSO based optimization technique of

proposed STSMC controller. Compared to the orientation angle and velocity response Fig. 10b of FOPID to the response of proposed system in a Fig. 9, it takes longer time to track the given linear reference trajectory and its error converges to zero after 0.0024 s time which is sluggish compared to STSMC error convergence time.

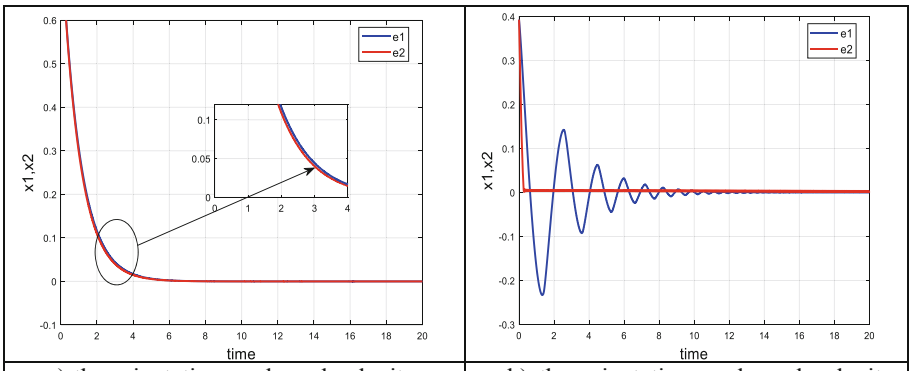

a) the orientation angle and velocity error response for linear trajectory of proposed STSMC controller

b) the orientation angle and velocity error response for linear trajectory of FOPID controller

Fig. 10. The orientation and velocity error response for linear trajectory $\delta_d = \pi/8$ of FOPID controller

5 Conclusions

This paper discusses the application of STSMC to autonomous ground vehicle systems. The lateral dynamics of a vehicle were simulated in this work using a simple two-degree-of-freedom bicycle model. Two distinct control algorithms were used to regulate the modified lateral motions. An investigation into the trajectory tracking control of autonomous ground vehicle systems used a super twisting sliding mode controller and a fractional order PID controller. A simulation was created using MATLAB/Simulink to test the effectiveness and performance of the controller. The controllers gain was optimized and tuned using the evolutionary algorithm and particle swarm optimization method. Finally, the findings show that the system tracks the needed trajectory with a minimal amount of tracking error. The suggested STSMC robustly monitors the supplied irregular reference environments, outperforming fractional order PID controllers in terms of performance. It is evident from the simulation results that the STSMC was used to control the orientation steering angle and velocity in order to stabilize the AGV system. The system's machine learning algorithm may be established in the future.

References

1. Amer, N.H., Zamzuri, H., Hudha, K., Kadir, Z.A.: Modelling and control strategies in path tracking control for autonomous ground vehicles: a review of state of the art and challenges. J. Intell. Rob. Syst. **86**(2), 225–254 (2016). https://doi.org/10.1007/s10846-016-0442-0

2. Chen, Q.: Studies in Autonomous Ground Vehicle Control Systems : Structure and Algorithms (2007)
3. Yousif, N., et al.: Control system design for autonomous vehicle path following and collision avoidance dissertation. J. Phys. Ther. Sci. **9**(1), 1–11 (2018). https://doi.org/10.1016/j.neuropsychologia.2015.07.010%0A. https://doi.org/10.1016/j.visres.2014.07.001%0A. https://doi.org/10.1016/j.humov.2018.08.006%0A. http://www.ncbi.nlm.nih.gov/pubmed/24582474%0A. https://doi.org/10.1016/j.gaitpost.2018.12.007%0A
4. Zamani, M., Karimi-Ghartemani, M., Sadati, N., Parniani, M.: Design of a fractional order PID controller for an AVR using particle swarm optimization. Control Eng. Pract. **17**(12), 1380–1387 (2009). https://doi.org/10.1016/j.conengprac.2009.07.005
5. Peng, J., Yu, J., Wang, J.: Robust adaptive tracking control for nonholonomic mobile manipulator with uncertainties. ISA Trans. **53**(4), 1035–1043 (2014). https://doi.org/10.1016/j.isatra.2014.05.012
6. Zhang, Y., Liu, G., Luo, B.: Finite-time cascaded tracking control approach for mobile robots. Inf. Sci. (Ny) **284**, 31–43 (2014). https://doi.org/10.1016/j.ins.2014.06.037
7. Zhuo-Yun, N., Yi-Min, Z., Qing-Guo, W., Rui-Juan, L., Lei-Jun, X.: Fractional-order PID controller design for time-delay systems based on modified bode's ideal transfer function. IEEE Access **8**, 103500–103510 (2020). https://doi.org/10.1109/ACCESS.2020.2996265
8. Normey-Rico, J.E., Alcalá, I., Gómez-Ortega, J., Camacho, E.F.: Mobile robot path tracking using a robust PID controller. Control Eng. Pract. **9**(11), 1209–1214 (2001). https://doi.org/10.1016/S0967-0661(01)00066-1
9. Lee, C.H., Chang, F.K.: Fractional-order PID controller optimization via improved electromagnetism-like algorithm. Expert Syst. Appl. **37**(12), 8871–8878 (2010). https://doi.org/10.1016/j.eswa.2010.06.009
10. Zhao, P., Chen, J., Song, Y., Tao, X., Xu, T., Mei, T.: Design of a control system for an autonomous vehicle based on adaptive-PID. Int. J. Adv. Robot. Syst. **9**, 1–11 (2012). https://doi.org/10.5772/51314
11. García-Sánchez, J.R., et al.: Tracking control for mobile robots considering the dynamics of all their subsystems: experimental implementation. Complexity **2017** (2017). https://doi.org/10.1155/2017/5318504
12. Maiti, D., Biswas, S., Konar, A.: Design of a fractional order PID controller using particle swarm optimization technique. ReTIS-08, pp. 1–5 (2008). http://arxiv.org/abs/0810.3776
13. Hoang, V.T., Pham, Q.H.: Adaptive super-twisting second-order sliding mode for attitude control of quadcopter UAVs. arXiv (2018)
14. Zhao, B., Wang, H., Li, Q., Li, J., Zhao, Y.: PID trajectory tracking control of autonomous ground vehicle based on genetic algorithm. In: Proceedings of the 31st Chinese Control Decision Conference, CCDC 2019, pp. 3677–3682 (2019). https://doi.org/10.1109/CCDC.2019.8832531
15. Dadras, S.: Path tracking using fractional order extremum seeking controller for autonomous ground vehicle. SAE Technical Paper, vol. 2017-March, no. March (2017). https://doi.org/10.4271/2017-01-0094
16. Gambhire, S.J., Kishore, D.R., Londhe, P.S., Pawar, S.N.: Review of sliding mode based control techniques for control system applications. Int. J. Dyn. Control **9**(1), 363–378 (2020). https://doi.org/10.1007/s40435-020-00638-7
17. Alam, W., Mehmood, A., Ali, K., Javaid, U., Alharbi, S., Iqbal, J.: Nonlinear control of a flexible joint robotic manipulator with experimental validation. J. Mech. Eng. **64**(1), 47–55 (2018). https://doi.org/10.5545/sv-jme.2017.4786
18. Hu, J., Zhang, Y., Rakheja, S.: Adaptive trajectory tracking for car-like vehicles with input constraints. IEEE Trans. Ind. Electron. **0046**(c) (2021). https://doi.org/10.1109/TIE.2021.3068672

19. Wu, Y., Wang, L., Zhang, J., Li, F.: Path following control of autonomous ground vehicle based on nonsingular terminal sliding mode and active disturbance rejection control. IEEE Trans. Veh. Technol. **68**(7), 6379–6390 (2019). https://doi.org/10.1109/TVT.2019.2916982
20. Dai, M., Qi, R., Cheng, X.: Super-twisting sliding mode control design for electric dynamic load simulator. In: Chinese Control Conference, CCC, vol. 2019-July, no. 1, pp. 3078–3083 (2019). https://doi.org/10.23919/ChiCC.2019.8865725
21. Shtessel, Y., Edwards, C., Fridman, L., Levant, A.: Sliding mode control and observation (2014)
22. Al-Mayyahi, A., Wang, W., Birch, P.: Design of fractional-order controller for trajectory tracking control of a non-holonomic autonomous ground vehicle. J. Control Autom. Electr. Syst. **27**(1), 29–42 (2015). https://doi.org/10.1007/s40313-015-0214-2